4K-bit and microlithographic integration of organic nonvolatile resistive memory devices

CrossMark

Younggul Song [a], Jingon Jang [a], Daekyoung Yoo [a], Seok-Heon Jung [b], Seunghun Hong [a], Jin-Kyun Lee [b], Takhee Lee [a,*]

[a] Department of Physics and Astronomy, Institute of Applied Physics, Seoul National University, Seoul 151-747, Republic of Korea
[b] Department of Polymer Science and Engineering, Inha University, Incheon 402-751, Republic of Korea

ARTICLE INFO

ABSTRACT

We demonstrated 4K-bit microscale organic nonvolatile resistive memory devices fabricated with a 10×10 μm^2 cell size in a 64×64 cross-bar array structure. This microscale integration was made via orthogonal photolithography processes using fluorinated photoresist and solvents and was achieved without causing damage to the underlying organic memory materials. Our microscale organic devices exhibited excellent memory performance that was retained more than 10 days with a high ON/OFF ratio ($>10^7$) and good endurance switching characteristics (>300 cycles). The demonstration of 4K-bit organic memory devices promises a possibility of highly-integrated microscale organic electronics applications.

© 2014 Elsevier B.V. All rights reserved.

1. Introduction

Organic material-based devices have recently received significant attention for their various advantages, including low manufacturing cost, large area processing capabilities, flexibility, and printing processes [1–6]. Due to these advantages, researchers have investigated a wide range of possible applications for these new devices, such as organic field effect transistors, organic light-emitting diodes, organic photovoltaic cells, organic sensors, and organic memories [3–9]. In particular, organic nonvolatile memory is considered to be a promising candidate for information storage devices because of its ease of fabrication, good performance, and durability [9–14]. Organic memory devices have often been fabricated in a cross-bar structure, which can realize high integration of memory cells [10–21].

However, the cross-bar structured organic memory devices have usually been limited to be less than a hundred bits integration with the individual cell size of several hundreds of microns (μm). The conventional photolithographic patterning technique to scale down the devices is difficult to apply to organic electronics because of the chemical incompatibility between organic electronic materials and organic solvents for photolithographic processing. Organic solvents (e.g., the developer used in lithography or acetone) dissolve not only the photoresist but also the organic electronic materials. Because of this issue, the majority of previous studies on organic electronic devices, including organic memory devices, have been restricted to non-lithographic fabrication methods, such as processes employing shadow masks or imprints [10–21]. This lithographic problem makes it difficult to integrate organic memory devices into a smaller device size at the micrometer scale. Other

---

* Corresponding author. Tel.: +82 2 880 4269; fax: +82 2 884 3002.
E-mail address: tlee@snu.ac.kr (T. Lee).

fabrication techniques for manufacturing organic memory devices that might overcome the scale-down problems have been studied, including nanowire pattern transfer, the direct metal-transfer method, and a method using photo cross-linkable organic memory [21–23]. However, because of their complicated processes, these methods may not be practical for high throughput, low-cost fabrication of delicate device structure, application to various memory materials and high integration of organic memory devices. For example, contact-based printing methods such as nanowire pattern transfer and direct metal-transfer method require a perfectly flat morphology in the bottom electrodes to prevent the disconnection of the transferred top metal lines. Application of photo cross-linkable organic memory is also limited to its crosslinking polymers due to its use of acetone.

To overcome the lithographic problem in organic electronics, some groups, including ours, have demonstrated a chemically non-damaging orthogonal photolithographic method that allows us to protect the underlying polymer organic films from the action of lithographic chemicals [24–27]. One possible solution is to use fluorinated photoresist (such as semi-perfluoroalkyl resorcinarene) and solvents (such as hydrofluoroethers) which are miscible to each other and orthogonal to most organic materials. These materials allow organic electronic devices to be fabricated at the microscale using the photolithography process [24,26].

In this study, we demonstrate the microfabrication of highly-integrated 4K-bit (64×64 array) organic nonvolatile resistive memory devices with a 10×10 μm^2 cell size, made possible by using fluorinated photoresist and solvents to avoid damaging the underlying organic memory materials. The fabricated organic memory devices exhibited a high ON/OFF ratio, stable switching characteristics, and excellent durability in terms of retention and endurance characteristics. Our devices showed a desirable operational uniformity and high device yield of operative memory distribution over the 4K-bit integration of organic memory devices.

2. Experimental

Fig. 1(a) illustrates the fabrication process for a 4K-bit microscale organic memory array using the orthogonal photolithographic method. For the fluorinated photoresist solution, 10 wt% of semi-perfluoroalkyl resorcinarene powder and 0.5 wt% of N-nonafluorobutanesulfonyloxy-1,8-naphthalimide photoacid generator were dissolved into a mixed solvent (3-ethoxy-1,1,1,2,3,4,4,5,5,6,6,6-dodecafluoro-2trifluoromethylhexane (HFE-7500): propylene glycol methyl ether acetate (PGMEA) = 4:1 weight ratio), and the solution was filtered through a 0.20-μm nylon syringe filter. For the active memory material (PI:PCBM), 2 ml of BPDA–PPD solution (10 wt% in NMP) and 0.3 ml of PCBM solution (0.5 wt% in NMP) were mixed and then diluted with 11.3 ml of NMP to control the active layer thickness. First, a SiO_2 (270 nm thick)/Si substrate was prepared and cleaned using acetone, isopropanol, and de-ionized water. The 20-nm-thick Al bottom

electrode lines with 10 μm line width were fabricated using conventional photolithography. To enhance the film uniformity, the Al bottom electrodes deposited on the SiO_2/Si substrate were exposed to UV-ozone for 10 min [14]. The prepared memory solution was spin coated onto the substrate, followed by soft-baking on a hot plate at 120 °C for 5 min in a N_2-filled glove box. Then the PI:PCBM layer was hard-baked on a hot plate at 300 °C for 30 min. Then, the fluorinated photoresist solution was spin coated, followed by baking process at 75 °C for 3 min under yellow light. Subsequently, the coated photoresist film was exposed under UV light (416 nm wavelength, intensity of ~ 8 mW/cm^2) through a photomask with 10 μm lines orthogonal to the bottom electrode lines. After post-exposure baking at 75 °C for 3 min, the photoresist film was developed by HFE-7200. Top electrodes of a 30 nm-thick Au layer were deposited on the developed samples. For the 4K-bit organic memory array devices, the sample was lifted off in an ethanol (5 vol%)-HFE-7200 (95 vol%) mixture to leave patterned Au electrodes on top of the PI:PCBM film. Fig. 1(b) shows the schematics and a cross-sectional transmission electron microscopy (TEM) image (right bottom inset) of the 4K-bit ($64 \times 64 = 4096$ bits) organic memory devices, which were fabricated with Al bottom electrodes and Au top electrodes on a Si substrate in the cross-bar structure. The width of the Al or Au electrodes was 10 μm and the interval between the Al or Au electrodes was 30 μm, which was defined with the microlithography process. More detailed fabrication procedures are provided in Supplementary Data (Fig. S1). A composite of polyimide (PI) and 6-phenyl-C61 butyric acid methyl ester (PCBM) was used as the active memory material due to its mechanical robustness and thermal stability [17–21]. The TEM image in Fig. 1(b) indicates the well-separated PI:PCBM active layer (~ 15 nm thick) between the Al (~ 25 nm thick) and Au (~ 30 nm thick) electrodes. Fig. 1(c) shows optical images of the 4K-bit microscale organic memory devices with a memory cell size of 10×10 μm^2, which were integrated in a 1.9×1.9 mm^2 region. In this study, semi-perfluoroalkyl resorcinarene (denoted as R_F-Calix-tBoc), a highly fluorinated chemical, was used as photoresist and 3-ethoxy-1,1,1,2,3,4,4,5,5,6,6,6,-dodecafluoro-2trifluoromethylhexane (denoted as HFE-7200) was used as developer. The chemical structures of all the chemicals used in this study (PI, PCBM, R_F-Calix-tBoc, and HFE-7200) are shown in Fig. 1(d). To verify the harmlessness of HFE-7200 to organic memory layers, the orthogonal property between PI:PCBM solution (N-methyl-2-pyrrolidone (NMP) as solvent) and organic solvent (acetone versus HFE-7200) was tested. The left picture in Fig. 1(e) shows that the PI:PCBM solution was completely dissolved in acetone, indicating that acetone will damage or dissolve the underlying PI:PCBM layer when used in photolithography. In contrast, the middle picture in Fig. 1(e) demonstrates that a good phase-separation was observed with PI:PCBM (upper layer) solution and HFE-7200 (lower layer). Furthermore, the right picture in Fig. 1(e) shows the insolubility of PCBM powder in HFE-7200. These results suggest that treatment with HFE-7200 will not damage the PI:PCBM layer when used in the orthogonal photolithography process.
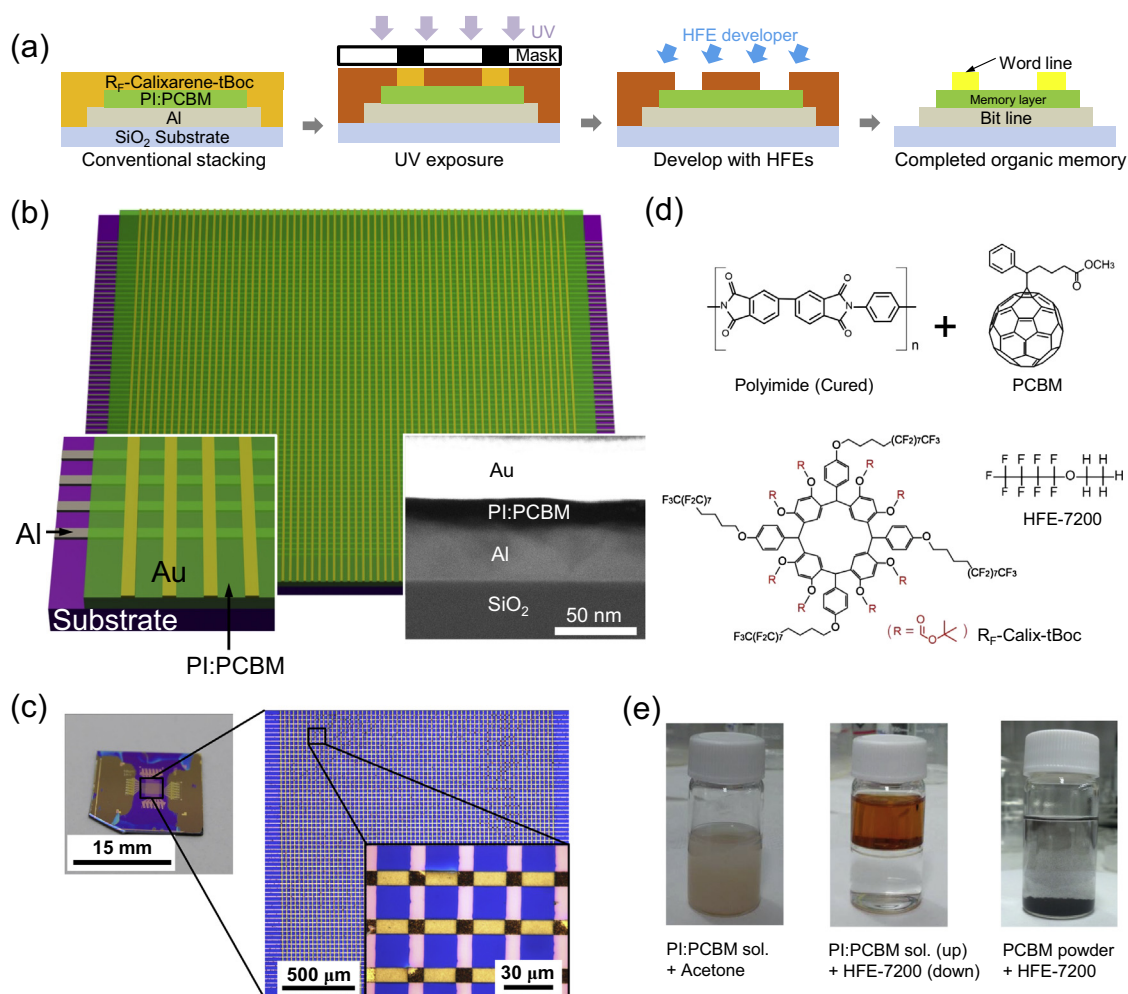
Fig. 1. (a) Schematics illustrating the microscale organic memory devices. (b) Schematic of the 4K-bit nonvolatile resistive organic memory devices on a Si substrate with a zoomed-in schematic (left bottom inset). Right bottom inset shows a cross-sectional TEM image of an organic memory cell. (c) Optical images of the fabricated 4K-bit organic memory devices. The line width of the electrodes is 10 μm. (d) Chemical structures of cured PI and PCBM used as the memory material together with those of semi-perfluoroalkyl resorcinarene and HFE-7200 used as the photoresist and developer, respectively. (e) Optical images of (left) the mixed solution of PI:PCBM and acetone, (middle) two phase-separated solutions of PI:PCBM and HFE-7200, and (right) PCBM powders, which sink to the bottom of HFE-7200.

3. Results and discussion

3.1. Electrical characteristics of microscale organic memory

Fig. 2(a) represents a current–voltage (I–V) graph of a memory cell in our devices. Here, the external voltage was applied to the Au top electrode while the Al bottom electrode was grounded. This particular memory cell (Fig. 2(a)) was turned on at 4.1 V (or at −3.7 V) and turned off at 10.6 V (or at −8.8 V) in the positive (or negative) voltage sweep, exhibiting typical nonvolatile and unipolar switching behavior. The electrical resistive switching can be explained by a charge-trapping mechanism (See Fig. S3 in Supplementary Data) [11,15,28–32]. For our memory devices, PCBM molecules embedded in the PI matrix seem to trap and release charge carriers [11,17–21,30–33], resulting in the bistable switching behavior. The ON/OFF ratio of the current level of LRS to that of

HRS was calculated from the data in Fig. 2(a) and is displayed in Fig. 2(b). Our microscale memory devices exhibited a high ON/OFF ratio (>10^6) within a ±4 V range. The I–V characteristics of our photolithographically fabricated organic memory devices (with a cell size of 10×10 μm^2) and the other organic memory devices made by the shadow mask method (with a cell size of 50×50 μm^2) were compared, as shown in Fig. 2(c). Both the memory devices showed similar memory switching behavior, such as abrupt current increase at the threshold voltages (V_{th}) at which the memory cells were switched on. The current level difference between these two types of memory devices can be explained by the cell size difference. We also observed potential multiple resistance states of our memory devices [18,34,35]. In Fig. 2(d), the first voltage sweep (double sweep between 0 and 7 V) switched the memory cell from the OFF to the ON state. The second voltage sweep (from 0 to 10 V) switched the cell into an inter-
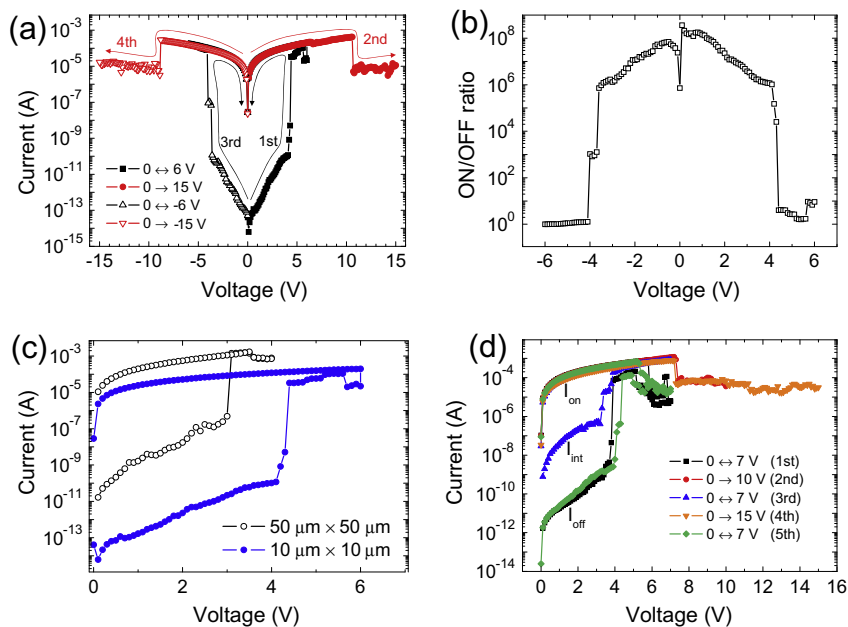
Fig. 2. (a) *I–V* characteristics of an organic memory device. (b) Current ON/OFF ratio for the memory cell as a function of the applied voltage. (c) Comparison of *I–V* curves for $50 \times 50 \ \mu m^2$–sized and $10 \times 10 \ \mu m^2$–sized memory cells. (d) Multi-level resistance states of the organic memory devices.

mediate state, as shown in the third sweep (double sweep between 0 and 7 V). The fourth sweep (from 0 to 15 V) switched the memory cell back to the OFF state. Results in Fig. 2 suggest that the memory devices fabricated by orthogonal photolithography properly operate without any intervention by fluorinated chemicals.

3.2. Device uniformity and data storage capability of 4K-bit organic memory devices

Fig. 3(a) includes a table summarizing the yield of our memory devices as well as a schematic showing the regions of the memory cells that were sampled for mea-
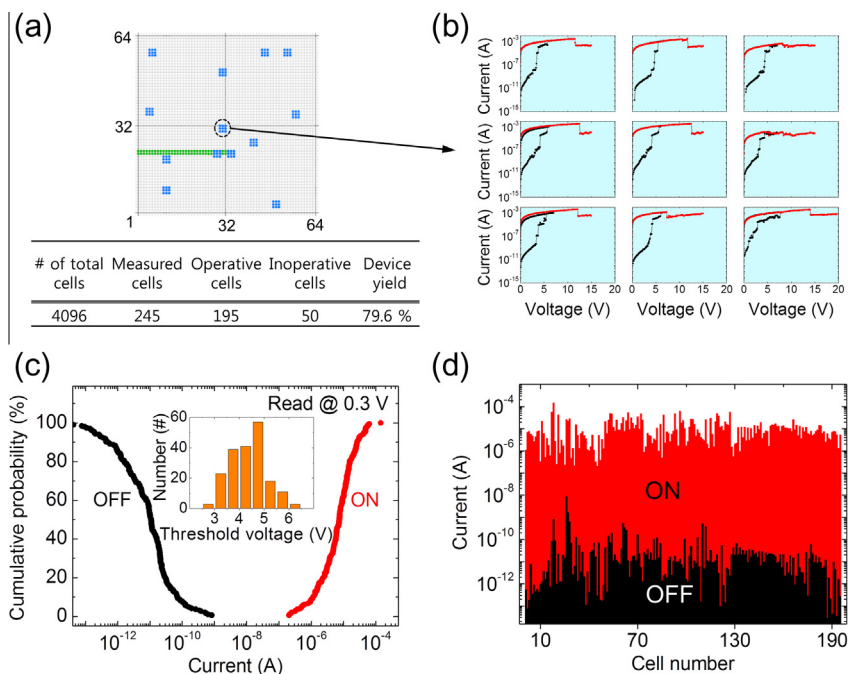
Fig. 3. (a) A schematic of the regions selected for measurement from the 4K-bit organic memory array and a table summarizing the device yield. (b) *I–V* curves measured from a selected region shown in (a). (c) Cumulative probability of ON and OFF currents for all operative memory cells (195 memory cells) and the threshold voltage distribution (inset). (d) Logarithmic representation of the ON and OFF currents of all operative memory cells.

surement. In the schematic, each blue square indicates a randomly chosen region of 3×3 memory cells that were measured, and the green rectangular region indicates 2×32 cells (8 bytes) that were measured. The locations of the blue square regions of the memory cells were intended to be evenly distributed on the 4K-bit organic memory devices to investigate the uniformity of the device. A number of other individually measured cells are not indicated in the schematic in Fig. 3(a). Among 4096 cells, a total of 245 cells were measured, and we found 195 cells were operating properly, corresponding to a device yield of ~80%. The device failures (50 inoperative cells) are related to electrode or dielectric breakdown and to deviation in the thickness of the organic layer (see Fig. S5 in Supplementary Data for failed cells).

In Fig. 3(b), all I–V characteristics of the memory cells from a blue-square region are shown. The I–V graphs are similar to each other in terms of the current level, V_{th}, and set/reset behaviors. Measuring each I–V characteristic on selected cell, we switched off measured cell to prevent cross-talk caused by nearby cells. To check the overall device operational uniformity, the current levels of the ON and OFF states were statistically analyzed for the 195 operative memory cells within the 4K-bit array (Fig. 3(c)). Our 4K-bit memory devices showed a well-defined margin between the current levels of LRS and those of HRS (over 10^2 in magnitude). Moreover, the 4K-bit memory devices showed a good distribution of threshold voltages, with values between 2.9 and 6.5 V, as shown in the inset of Fig. 3(c). Fig. 3(d) displays the statistical distribution of ON/OFF current levels in a logarithmic scale for the 195 operative memory cells. The majority of the mem-

ory cells exhibited a large difference in order (~10^6) between the current levels of LRS (~10^{-6} A) and HRS (~10^{-12} A).

To investigate the memory storage durability, a retention test was performed on our memory devices (Fig. 4(a)). First, the current levels of LRS and HRS were measured for 2×10^4 s with a measurement interval, Δt, of 10 s and a read voltage of 0.3 V. After 10 days of storage in a glove box filled with N_2 gas, the same device was again subjected to retention measurement, this time for 2×10^3 s. In this second retention test, the ON/OFF current ratios held at ~10^7 in magnitudes and did not exhibit any serious electrical degradation even 10 days after the first retention test. Fig. 4(b) shows the DC sweep endurance test used to investigate the switching performance of our organic memory devices. DC voltage sweeps were applied to the memory device, turning it on and off repeatedly and sequentially. Although some variations of OFF-current level were observed, the memory device maintained a high ON/OFF ratio of over 10^4 during 300 repeated switching cycles. The increase of OFF current might be due to the accumulation of charge by continuous set/reset process. This limit could be improved by tuning of V_{set}/V_{reset} ratio.

4. Conclusions

In summary, we fabricated 4K-bit highly integrated and microscale resistive nonvolatile organic memory devices with a 10×10 μm^2 cell size in a 64×64 cross-bar array structure. The fabrication of 4K-bit and microscale devices was made possible by the use of fluorinated organic materials and solvents in the orthogonal photolithography process. Our 4K-bit organic memory devices also exhibited good device operation performance in terms of uniformity, retention, and endurance characteristics. This study may foster microscale organic electronics applications for high-capacity information storage.

Appendix A. Supplementary material

Supplementary data associated with this article can be found, in the online version, at http://dx.doi.org/10.1016/j.orgel.2014.12.008.
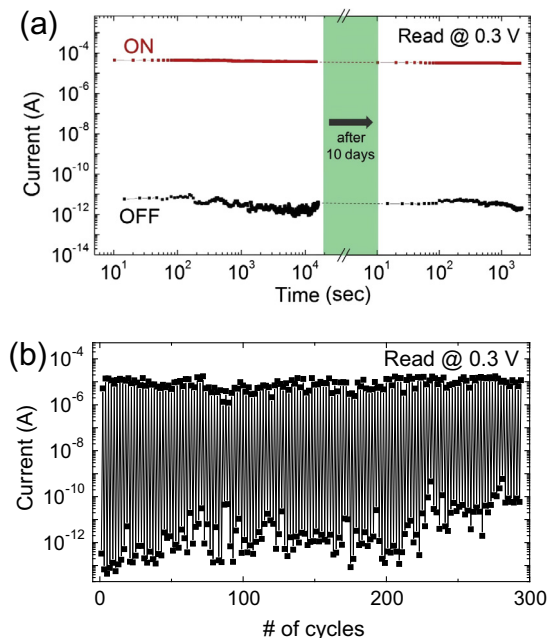
Fig. 4. (a) Retention time and (b) DC sweep endurance test results for the 4K-bit organic memory devices. Retention time was retested 10 days after the first retention time test was performed.

References

[1] J. Heeger, S. Kivelson, J.R. Schrieffer, W.P. Su, Rev. Mod. Phys. 60 (1988) 781.
[2] S.R. Forrest, Nature 428 (2004) 911.
[3] M. Muccini, Nat. Mater. 5 (2006) 605.
[4] L. Briseno, S.C.B. Mannsfeld, M.M. Ling, S. Liu, R.J. Tseng, C. Reese, M.E. Roberts, Y. Yang, F. Wudl, Z. Bao, Nature 444 (2006) 913.
[5] H. Yan, Z. Chen, Y. Zheng, C. Newman, J.R. Quinn, F. Dotz, M. Kastler, A. Facchetti, Nature 457 (2009) 679.
[6] T. Sekitani, H. Nakajima, H. Maeda, T. Fukushima, T. Aida, K. Hat, T. Someya, Nat. Mater. 8 (2009) 494.
[7] M. Segal, M. Singh, K. Rivoire, S. Difley, T.V. Voorhis, M.A. Baldo, Nat. Mater. 6 (2007) 374.
[8] G. Schwartz, B.C. Tee, J. Mei, A.L. Appleton, H. Kim do, H. Wang, Z. Bao, Nat. Commun. 4 (2013) 1859.
[9] J. Ouyang, C.W. Chu, C.R. Szmanda, L. Ma, Y. Yang, Nat. Mater. 3 (2004) 918.
[10] Y. Yang, J. Ouyang, L. Ma, R.J.-H. Tseng, C.-W. Chu, Adv. Funct. Mater. 16 (2006) 1001.
[11] J.C. Scott, L.D. Bozano, Adv. Mater. 19 (2007) 1452.
[12] Q.-D. Ling, D.-J. Liaw, C. Zhu, D.S.-H. Chan, E.-T. Kang, K.-G. Neoh, Prog. Plolym. Sci. 33 (2008) 917.
[13] Cho, S. Song, Y. Ji, T.-W. Kim, T. Lee, Adv. Funct. Mater. 21 (2011) 2806.
[14] Y. Ji, D.F. Zeigler, D.S. Lee, H. Choi, A.K.-Y. Jen, H.C. Ko, T.-W. Kim, Nat. Commun. 4 (2013) 2707.
[15] L.D. Bozano, B.W. Kean, M. Beinhoff, K.R. Carter, J.C. Scott, Adv. Funct. Mater. 15 (2005) 1933.
[16] K. Asadi, M. Li, N. Stingelin, P.W.M. Blom, D.M. de Leeuw, Appl. Phys. Lett. 97 (2010) 193308.
[17] S. Song, B. Cho, T.-W. Kim, Y. Ji, M. Jo, G. Wang, M. Choe, Y.H. Kahng, H. Hwang, T. Lee, Adv. Mater. 22 (2010) 5048.
[18] Cho, T.-W. Kim, S. Song, Y. Ji, M. Jo, H. Hwang, G.-Y. Jung, T. Lee, Adv. Mater. 22 (2010) 1228.
[19] Y. Ji, B. Cho, S. Song, T.-W. Kim, M. Choe, Y.H. Kahng, T. Lee, Adv. Mater. 22 (2010) 3071.
[20] S. Song, J. Jang, Y. Ji, S. Park, T.-W. Kim, Y. Song, M.-H. Yoon, H.C. Ko, G.-Y. Jung, T. Lee, Org. Electron. 14 (2013) 2087.
[21] J.J. Kim, B. Cho, K.S. Kim, T. Lee, G.Y. Jung, Adv. Mater. 23 (2011) 2104.
[22] J.E. Green, J.W. Choi, A. Boukai, Y. Bunimovich, E. Johnston-Halperin, E. Delonno, Y. Luo, B.A. Sheriff, K. Xu, Y.S. Shin, H.-R. Tseng, J.F. Stoddart, J.R. Heath, Nature 445 (2007) 414.
[23] K. Wei Lek, R.J. Tseng, W. Wei, P. Qibing, Y. Yang, Presented at Proc, IEEE int. Electron Dev. Meet. 12 (2007).
[24] A. Zakhidov, J.-K. Lee, H.H. Fong, J.A. DeFranco, M. Chatzichristidi, P.G. Taylor, C.K. Ober, G.G. Malliaras, Adv. Mater. 20 (2008) 3481.
[25] J.-K. Lee, M. Chatzichristidi, A.A. Zakhidov, P.G. Taylor, J.A. DeFranco, H.S. Hwang, H.H. Fong, A.B. Holmes, G.G. Malliaras, C.K. Ober, J. Am. Chem. Soc. 130 (2008) 11564.
[26] A. Zakhidov, J.-K. Lee, J.A. DeFranco, H.H. Fong, P.G. Taylor, M. Chatzichristidi, C.K. Ober, G.G. Malliaras, Chem. Sci. 2 (2011) 1178.
[27] Y. Ouyang, J.-K. Lee, M.E. Krysak, J. Sha, C.K. Ober, J. Mater. Chem. 22 (2012) 5746.
[28] Rose, Phys. Rev. 97 (1955) 1538.
[29] J.G. Simmons, R.R. Verderber, Proc. R. Soc. Lond. A 301 (1967) 77.
[30] L.D. Bozano, B.W. Kean, V.R. Deline, J.R. Salem, J.C. Scott, Appl. Phys. Lett. 84 (2004) 607.
[31] Carbone, B.K. Kotowska, D. Kotowski, Phys. Rev. Lett. 95 (2005) 23660.
[32] T.-W. Kim, S.-H. Oh, H. Choi, G. Wang, H. Hwang, D.-Y. Kim, T. Lee, IEEE. Elecron. Dev. Lett. 29 (2008) 852.
[33] Laiho, H.S. Majumdar, J.K. Baral, F. Jansson, R. Österbacka, O. Ikkala, App. Phys. Lett. 93 (2008) 203309.
[34] J.G. Park, W.S. Nam, S.H. Seo, Y.G. Kim, Y.H. Oh, G.S. Lee, U.G. Paik, Nano Lett. 9 (2009) 1713.
[35] G. Yang, H.-Y. Chen, L. Ma, Y. Shao, Y. Yang, Appl. Phys. Lett. 95 (2009) 203506.